PHYSICAL REVIEW E **88**, 020201(R) (2013)

Spatially modulated kinks in shallow granular layers

J. E. Macías, M. G. Clerc, C. Falcón,* and M. A. García-Ñustes
Departamento de Física, Facultad de Ciencias Físicas y Matemáticas, Universidad de Chile, Casilla 487-3, Santiago, Chile

(Received 5 April 2013; revised manuscript received 30 June 2013; published 19 August 2013)

We report on the experimental observation of spatially modulated kinks in a shallow one-dimensional fluidized granular layer subjected to a periodic air flow. We show the appearance of these solutions as the layer undergoes a parametric instability. Due to the inherent fluctuations of the granular layer, the kink profile exhibits an effective wavelength, *a precursor*, which modulates spatially the homogeneous states and drastically modifies the kink dynamics. We characterize the average and fluctuating properties of this solution. Finally, we show that the temporal evolution of these kinks is dominated by a hopping dynamics, related directly to the underlying spatial structure.

DOI: 10.1103/PhysRevE.88.020201 PACS number(s): 45.70.Qj, 05.45.−a, 47.20.Ky, 47.54.−r

Macroscopic systems under the influence of injection and dissipation of quantities such as energy and momentum usually exhibit coexistence of different states, which is termed *multistability* [1–3]. Heterogeneous initial conditions—usually caused by the inherent fluctuations—generate spatial domains which are separated by their respective interfaces. These interfaces are known as fronts [2]. The evolution of these solutions can be regarded as a particle-type one, i.e., they can be characterized by a set of continuous parameters such as the position, width, charge, and so forth. In the particular case where fronts separate symmetric states, these front solutions are termed *kinks*. Usually, these types of structures have been studied in regimes where the symmetric states are homogeneous ones [2]. Kinks have been a central element in classical and quantum field theory to understand the dynamics and evolution of several physical systems [4]. In parametrically driven systems this type of structure appears through instabilities which lead to the emergence of symmetric states which are out of phase by half the period of the forcing [5]. A typical example of such systems are vertically vibrofluidized two-dimensional granular layers where kink solutions have naturally been observed (see references in Ref. [6] therein). Although several studies have been performed in two-dimensional fluidized granular layers, only a handful of studies on one-dimensional fluidized granular layers where kinks connecting homogeneous states have been reported experimentally [7,8] and numerically [9,10]. Furthermore, to our knowledge, there is no observation of kink solutions connecting spatially modulated states [11], which can strongly influence their stability, bifurcation diagrams, and dynamical properties.

The aim of this Rapid Communication is to report the observation of kink solutions connecting spatially modulated states. The system under study is a one-dimensional shallow granular layer fluidized by periodic air flow (cf. Fig. 1). Air flows have already been used to study pattern formation in fluidized granular layers in one- [12] and two- [13] dimensional systems. Here, we show experimentally the emergence of kink solutions as the layer undergoes a parametric instability, and characterize its average and fluctuating properties. Its profile displays spatial oscillations on the homogeneous state induced by intrinsic fluctuations of the system. These oscillations dictate the temporal evolution of the kink, which is a hopping one, much similar to a Brownian particle in a periodic potential [14,15].

Experimental setup. The experimental setup under study is displayed in Fig. 1. A cell (width $L = 200$ mm, height $H = 200$ mm, and depth $D = 3.5$ mm) made out of two large glass walls with a horizontally placed thick-band-like sponge (6 mm thick, 200 mm wide, and 15 mm tall) acts as a porous floor where approximately 25 000 monodisperse bronze spheres (diameter $a = 350\ \mu$m) are deposited. In grain diameter units, the granular layer is $570a$ wide, $10a$ deep, and $5a$ tall. D is not changed in these experiments in order to treat the interface dynamics as a quasi-one-dimensional one. Thin rods of plexiglass were introduced vertically between the glass walls effectively shortening L to study the dynamics of a reduced granular layer, which we will explain below.

The excitation system of the granular layer is similar to the one described in [12], where a periodic air flow is generated by an air compressor (Indura Huracán 1520) and regulated by an electromechanical proportional valve (Teknocraft 203319), a precision control regulator (Controlair 100), and an air lung. The valve aperture is set by a variable voltage signal controlled by the first output of a two-channel function generator (RIGOL DG1022) through a power amplifier (NF model HFA4011). A symmetrical triangular signal with frequency f_o and a nonzero offset is used to generate through the air flow a time-modulated controllable pressure signal, as shown in the inset of Fig. 1(a). Pressure oscillations are measured 50 cm before the flow enters the cell with a dynamic pressure sensor (PCB 106B) and a signal conditioner (PCB 480C02). We have checked experimentally the linearity between the peak voltage delivered by the function generator and the peak pressure fluctuations P_o at the forcing frequency f_o. Hence, the control parameters are f_o and P_o. We have also checked that the extra pressure drop due to the motion and fluidization of the granular layer is negligible with respect to the one measured on the unloaded cell.

Images of the granular bed motion are acquired with a CCD camera over a 100 s time window in a 1080×200 px spatial window (0.19 mm/px sensitivity in the horizontal direction and 0.18 mm/px in the vertical direction). For each

*cfalcon@ing.uchile.cl

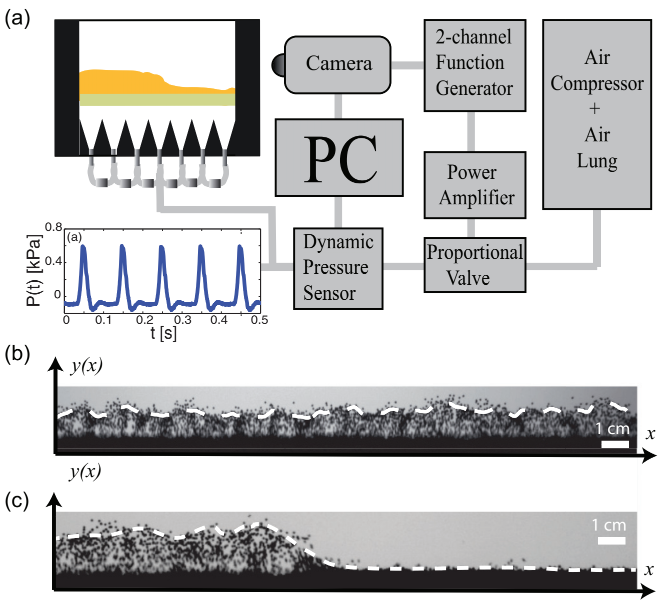

FIG. 1. (Color online) (a) Experimental setup. The inset depicts a typical temporal trace of the pressure fluctuations. (b) Typical image of the excited granular layer. The dashed white line corresponds to the numerically calculated granular interface $y(x)$. (c) Granular surface kink on shallow granular layers.

experimental configuration, two image sequences are taken. The first one, acquired at high frame rate (100 fps), is used to study the typical oscillation frequencies of the granular layer. The second one, set at the subharmonic frequency $f_o/2$ using the second output of the function generator as a trigger, is used to ensure a stroboscopic view of the oscillating layer. The granular interface $y(x,t)$ is tracked for every point in space x at each time t using a simple threshold intensity algorithm (see Ref. [12] for more information), as shown in Fig. 1. To do this, white light is sent through a diffusing screen from behind the granular layer as images are taken from the front, enhancing contrast and thus surface tracking algorithms. Figure 1 shows a snapshot of the granular layer and a kink solution using the above mentioned tracking algorithm.

Experimental results. We have conducted experiments in the parameter space of peak pressures P_o ranging from 100 Pa to 10 kPa and excitation frequencies f_o ranging from 5 to 20 Hz. We have concentrated our studies in the frequency range $f_o \in [12.5,14.5]$ Hz, as the phenomenology is quite reproducible and less input pressure is needed. We have restricted our experimental cell, shortening L to 5 cm, in order to study the dynamics of the homogeneous state, preventing the appearance of kinks which form for larger widths.

As we increase P_o for a fixed excitation frequency f_o, the granular bed displays small surface fluctuations (less than a diameter) of the upper layer of grains. This motion is enhanced as P_o increases, lifting the complete layer over a period of the pressure fluctuations. For a critical value of $P_o = P_o^c$, the flat oscillating layer becomes unstable to small perturbations through a parametric instability, displaying subharmonic oscillations at $f_o/2$. Therefore, the granular layer presents an effective parametric resonance as a consequence of the forcing [16]: The periodic air flow is responsible for inducing the oscillatory behavior of the layer and its respective parametric resonance. This subharmonic response can be observed by measuring the space averaged motion

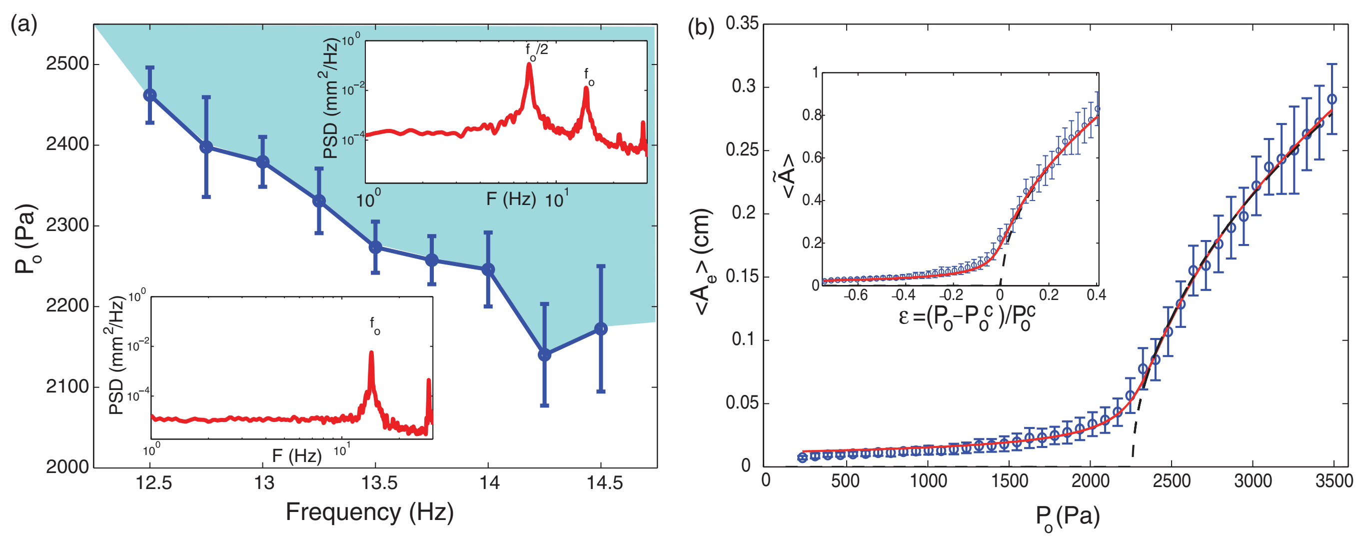

FIG. 2. (Color online) (a) Parametric instability curve. The continuous line shows the experimentally computed phase line P_o^c as a function of f_o. For $P_o < P_o^c$ only harmonic oscillations of the flat layer are present in the reduced cell ($L = 5$ cm). For $P_o > P_o^c$ subharmonic oscillations are dominant, arising from a parametric instability. Lower inset: power spectral density (PSD) of the flat layer harmonic oscillations at $f_o = 14$ Hz for $P_o = 1520 \pm 20$ Pa. Upper inset: PSD of the dominant subharmonic oscillations of the flat layer at $f_o/2 = 7$ Hz for $P_o = 3840 \pm 20$ Pa. (b) Bifurcation diagram for the subharmonic amplitude $\langle A_e \rangle$ vs P_o for $f_o = 14$ Hz. Dashed line is the theoretical prediction for $\langle A_e \rangle = \alpha^{1/2}(P_o - P_o^c)^{1/2}$ where $\alpha = 33.64 \pm 1.16\times$ cm^2/kPa is a calibration factor and $P_o^c = 2247 \pm 39$ Pa. The continuous line is a theoretical fit of $\langle A_e \rangle = \alpha\{(P_o - P_o^c) + [(P_o - P_o^c)^2 + 2\tilde{\eta}]^{1/2}/2\}^{1/2}$ where $\tilde{\eta} = 9264 \pm 2913$ Pa^2 is the noise intensity. Inset: Normalized amplitude $\langle \tilde{A} \rangle = \langle A_e \rangle / \alpha\sqrt{P_o^c}$ vs $\epsilon = (P_o - P_o^c)/P_o^c$. The dashed line follows the prediction $\tilde{A} = \epsilon^{1/2}$. The continuous line is a theoretical fit of $\langle \tilde{A} \rangle = \{[\epsilon + (\epsilon^2 + 2\eta)^{1/2}]/2\}^{1/2}$, where η is the normalized noise intensity.

of homogeneous granular interface $y(x,t)$, that is, $Y(t) = L^{-1}\int_0^L y(x,t)dx$ as a function of time t. For small P_o the power spectral density of $Y(t)$ displays a peak at f_o showing the harmonic character of the oscillation (cf. Fig. 2, lower inset). As P_o is increased, a subharmonic oscillation appears [cf. Fig. 2(a), upper inset]. For each excitation frequency there is a transition from harmonic to subharmonic dominant oscillations of the flat layer as P_o surpasses a critical value P_o^c, which is displayed by the continuous line in Fig. 2(a). This transition is found to be smooth and supercritical in nature for all $f_o \in [12.5,14.5]$ Hz. For the sake of simplicity in what follows f_o will be fixed at 14 Hz. It must be noticed that increasing H from $5a$ to $10a$ will change this dynamical state, as a patterned state appears [12].

To characterize the transition pressure P_o^c, we follow the scheme proposed in [17]. We compute the bifurcation diagram of the envelope A_e of subharmonic oscillations of $Y(t)$, $A_e \cos(\pi f_o t)$, as P_o is increased. From the temporal trace of the layer oscillations the harmonic part is filtered out and the amplitude of the remaining subharmonic oscillations is computed using a Hilbert transform algorithm [18]. The bifurcation diagram is shown in Fig. 2(b), where the temporal average of A_e, $\langle A_e\rangle$, is plotted versus P_o. The error bars correspond to the standard deviation of the values of the envelope $\sigma_A = \sqrt{A_e^2 - \langle A_e\rangle^2}$. The smooth bifurcation curve can be described with a simple model which takes into account noise in a supercritical transition [17]. Thus, we can compute the threshold value of P_o^c for each excitation frequency f_o, and the intensity of the noise η of the layer fluctuations following the expression $\langle A_e\rangle = \alpha\sqrt{[(P_o - P_o^c) + \sqrt{(P_o - P_o^c)^2 + 2\tilde{\eta}}]/2}$, where $\tilde{\eta}$ is the noise intensity and α is a calibration factor. For every f_o in our experiments, all bifurcation curves follow the above expression.

The spatial structure of the granular layer was also studied to characterize the stationary states as the layer oscillates. For $P_o < P_o^c$, the harmonically oscillating flat layer displays no typical spatial scale. For $P_o > P_o^c$, fluctuations of the flat layer display a characteristic wavelength and frequency sporadically [see Fig. 1(b)], disappearing randomly with a typical lifetime, which is known as a *precursor* [19]. This phenomenon is a consequence of the balance between energy injection, caused by internal fluctuations of the granular layer, and the local dissipation of the slowest decaying spatial mode of the uniform steady state of the layer interface. In our experimental setup, the typical wavelength λ of the precursor is typically $\sim$2 cm, which is of the order of $60a$. We have checked that λ is independent of the periodicity or the position of the air inlets. No discernible change is observed for our experimental control parameters. λ can be understood as the typical wavelength of a secondary spatial instability which occurs for larger pressures than the ones reported here. It must be noticed that this type of supercritical noisy bifurcation has also been observed in vibrofluidized granular layers, although the analysis of the transition was performed via spectral properties of the fluctuations [20].

Now, we will concern ourselves with kinks appearing through the above described transition in the extended cell for $L = 20$ cm. Maintaining f_o at 14 Hz and increasing $\varepsilon = (P_o - P_o^c)/P_o^c$ above the transition, the subharmonic motion described above allows the system to exhibit bistability between two states which are out of phase and, thus, a spatial connection between them. More precisely, there is a height jump as we go from left to right through a finite region of the layer where this shift occurs. This means that, at any given instant, on one side of the region the granular layer is moving upwards and on the other side it is moving downwards.

A kink can appear in any point of the experimental cell spontaneously. By choosing the phase mismatch between the triggering signal and the layer oscillation, we can image the kink when the separation between the in-phase and out-of-phase parts of the oscillating granular layer is at its maximum. Averaging over all the computed interfaces in an image sequence, we calculate the averaged front, its height d, and width Δ for different ε, as shown in Fig. 3. Here, $2d$ corresponds to the distance between the in- and out-of-phase states, measured at its maximum separation. Δ is computed as the average width of the spatial derivative of the kink solution. The error bars correspond to the standard deviation of d and Δ. We can see that d grows linearly with ε and Δ is roughly constant at 0.7 cm (independent of ε). Note that the computed kink displays a spatial modulation on both connected states, as discussed above. Thus, its typical wavelength is again λ (cf. Fig. 3). Further increasing the number of images used in the average values of d, Δ, and λ does not affect the computed values.

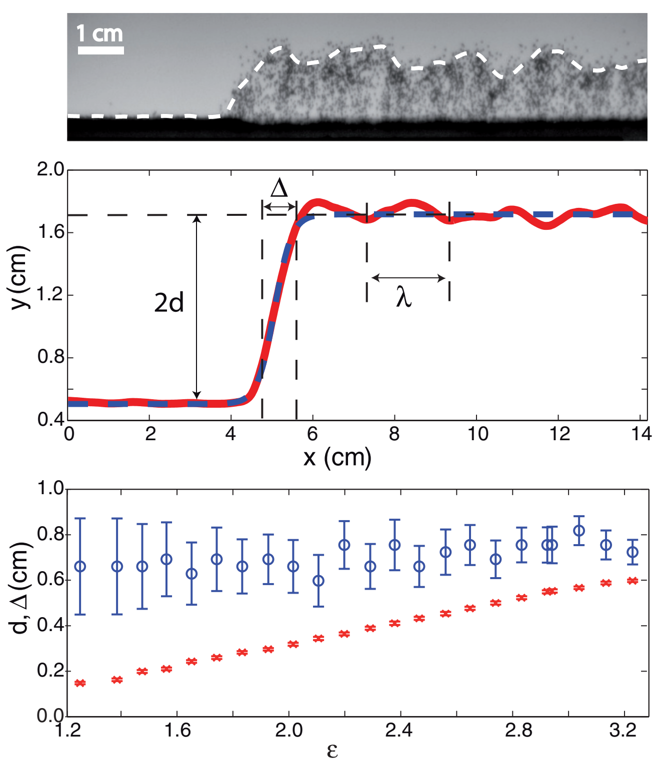

FIG. 3. (Color online) Top: Typical image of a granular kink at $P_o = 8038 \pm 20$ Pa ($\varepsilon = 2.42 \pm 0.01$). The dashed line is the numerical interface detection. Middle: Granular kink averaged over 1000 frames. d stands for the granular kink height with respect to the middle plane and Δ stands for the typical core size of the kink. Bottom: Granular kink height d ($\times$) and typical core size Δ ($\circ$) as a function of ε. Error bars stand for the standard deviation for d and Δ for each value of ε.

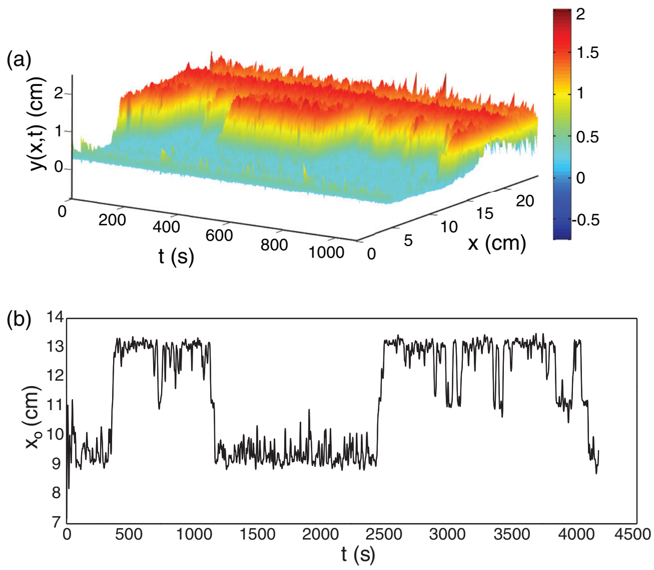

FIG. 4. (Color online) Motion of the granular kink. (a) Image sequence of 20 min of $P_o = 8038 \pm 20$ Pa ($\varepsilon = 2.42 \pm 0.01$). (b) Temporal trace of the core of the kink $x_o(t)$ as a function of time.

The long term dynamics of the spatially modulated kink are dictated by its structure and inherent fluctuations. A typical image sequence of the kink motion acquired over long time periods ($\sim 10^4$ periods of oscillation) is depicted in Fig. 4(a), where the complete structure shifts its position in the experimental cell through discrete jumps. This motion is tracked in time by following the kink position, $x_o(t)$, which is the position in space where the spatial derivative of the kink reaches its maximum. The typical distance between these jumps is λ [cf. Fig. 4(b)] and they occur at random times either to the left or the right of the cell. Although the kink displays these jumps, the temporal average of $x_o(t)$, $\langle x_o \rangle$, does not change in the experimental observation time. Hence, the dynamics of $x_o(t)$ can be understood as a random motion (where fluctuations come from the inherent noise of the granular layer) within a periodical potential (arising from the spatial structure of the precursor) [14]. It can be foreseen that in the case of the existence of a small asymmetry in the system (for instance, tilting the cell) the evolution of the kink could resemble that of a Brownian-type motor [15,21], but this is only an extrapolation of the previous dynamics and needs experimental confirmation.

In summary, we have studied the stability properties and bifurcation diagrams of kink solutions in a shallow one-dimensional fluidized granular layer subjected to a periodic air flow. The inherent noise of the system simultaneously induces fluctuations on the kink position, and sustains an effective pattern over the extended homogeneous state. These ingredients combined allow us to figure out the long time dynamics of the kink solution as a Brownian-type motor. A deeper understanding on the existence, properties, dynamics, and interaction of kinks is still lacking. Theoretical and experimental work in this direction is in progress.

Acknowledgments. The authors would like to thank an anonymous referee for his constructive criticism towards our work. We acknowledge financial support from ANR-CONICYT 39 and ACT127. M.G.C., C.F., and M.A.G.-N. are grateful for the financial support of FONDECYT projects 1120320, 1130354, and 3110024, respectively.

[1] G. Nicolis and I. Prigogine, *Self-Organization in Non Equilibrium Systems* (Wiley, New York, 1977).
[2] L. M. Pismen, *Patterns and Interfaces in Dissipative Dynamics*, Springer Series in Synergetics (Springer, Berlin, 2006).
[3] M. C. Cross and P. C. Hohenberg, Rev. Mod. Phys. **65**, 851 (1993).
[4] N. Manton and P. Sutcliffe, *Topological Solitons* (Cambridge University Press, Cambridge, 2004).
[5] L. D. Landau and E. M. Lifshiftz, *Mechanics* (Pergamon, Oxford, 1976).
[6] I. Aronson and L. Tsimring, *Granular Patterns* (Oxford University Press, New York, 2009).
[7] S. Douady, S. Fauve, and C. Laroche, Europhys. Lett. **8**, 621 (1989).
[8] S. J. Moon, M. D. Shattuck, C. Bizon, D. I. Goldman, J. B. Swift, and H. L. Swinney, Phys. Rev. E **65**, 011301 (2001); S. J. Moon, D. I. Goldman, J. B. Swift, and H. L. Swinney, Phys. Rev. Lett. **91**, 134301 (2003).
[9] Z. Peng, M. Guo-Qing, H. Kai, Y. Yi, and W. Rong-Jue, Chin. Phys. Lett. **22**, 1961 (2005).
[10] C. Hui, C. Wei-Zhong, and M. Guo-Qing, Chin. Phys. Lett. **30**, 044501 (2013).
[11] P. Coullet, Int. J. Bif. Chaos **12**, 245 (2002).
[12] I. Ortega, M. G. Clerc, C. Falcón, and N. Mujica, Phys. Rev. E **81**, 046208 (2010).
[13] J. Li, I. S. Aranson, W. K. Kwok, and L. S. Tsimring, Phys. Rev. Lett. **90**, 134301 (2003).
[14] H. Risken, *The Fokker-Planck Equation* (Springer-Verlag, Berlin, 1984).
[15] P. Reiman and P. Hanggi, Appl. Phys. A **75**, 169 (2002).
[16] M. G. Clerc, C. Falcón, C. Fernandez-Oto, and E. Tirapegui, Europhys. Lett. **98**, 30006 (2012).
[17] G. Agez, M. G. Clerc, and E. Louvergneaux, Phys. Rev. E **77**, 026218 (2008).
[18] A. V. Oppenheim and R. W. Schafer, *Digital Signal Processing* (Prentice Hall, New Jersey, 1975).
[19] W. Schöpf and W. Zimmermann, Phys. Rev. E **47**, 1739 (1993).
[20] D. I. Goldman, J. B. Swift, and H. L. Swinney, Phys. Rev. Lett. **92**, 174302 (2004).
[21] M. G. Clerc, C. Falcón, and E. Tirapegui, Phys. Rev. Lett. **94**, 148302 (2005); Phys. Rev. E **74**, 011303 (2006).